Photonic crystals composed of virtual pillars with magnetic walls: Photonic band gaps and double Dirac cones

Seong-Han Kim,* Soeun Kim, and Chul-Sik Kee†
Integrated Optics Laboratory, Advanced Photonics Research Institute, GIST, Gwangju 61005, Republic of Korea
(Received 7 June 2016; revised manuscript received 19 July 2016; published 11 August 2016)

Photonic crystals composed of virtual pillars with magnetic walls are proposed. A virtual pillar with a magnetic wall can be created inside a parallel perfect electric conductor plate waveguide by introducing a circular perfect magnetic conductor patch in the upper perfect electric conductor plate of the waveguide. The virtual pillar mimics a perfect magnetic conductor pillar with a radius less than that of the circular patch because electromagnetic waves can slightly penetrate the wall. Furthermore, the photonic band structures of a triangular photonic crystal composed of virtual pillars for the transverse electromagnetic modes of the waveguide are investigated. They are very similar to those of a triangular photonic crystal composed of infinitely long perfect electric conductor cylinders for transverse magnetic modes. The similarity between the two different photonic crystals is well understood by the boundary conditions of perfect electric and magnetic conductor surfaces. A double Dirac cone at the center of the Brillouin zone is observed and thus the virtual pillar triangular photonic crystal can act a zero-refractive-index material at the Dirac point frequency.

DOI: 10.1103/PhysRevB.94.085118

I. INTRODUCTION

It is well known that a perfect electric conductor (PEC) completely reflects electromagnetic (EM) waves with reflection phase of 180°. There is a conceptual material, termed a perfect magnetic conductor (PMC), on which the tangential component of a magnetic field is absent; therefore, it can reflect an electromagnetic wave with no phase change. Since PMCs are both beneficial and practical as antenna ground planes, small flat signal processing filters, or filters as part of waveguide structures, and artificial structures that act as PMCs, such as a high impedance ground plane and an uniplanar compact photonic band gap (PBG) structure, have been proposed, although their acting frequency ranges are very narrow [1–4]. Recently it has been proposed that a corrugated PMC surface can support spoof surface magnon polaritons, similar to how a corrugated PEC surface can support spoof surface plasmon polaritons [5–7].

The combination of PEC and PMC plates can give rise to interesting EM phenomena. For example, a parallel configuration of PEC and PMC plates cannot support transverse electromagnetic (TEM) modes between the plates while two parallel PEC plates can; the latter configuration is known as a parallel plate waveguide (PPW). A virtual magnetic wall to block TEM modes can be formed by combining PPW and parallel PEC/PMC plates because TEM modes propagating in a PPW are completely reflected at the interface between PPW and parallel PEC/PMC plates. From the idea of the virtual magnetic wall, a virtual magnetic scatterer could be proposed. For example, introducing a circular PMC patch in the upper PEC plate of a parallel PEC plate waveguide would form a cylindrical virtual magnetic wall under the patch. It is expected that the cylindrical virtual magnetic wall scatters EM waves propagating in the waveguide, as is the case of a pillar. If the virtual magnetic wall under the PMC patch can act as a pillar in the waveguide, the introduction of a periodic array of circular PMC patches can create a photonic crystal (PC) of virtual pillars in the waveguide. PCs composed of virtual pillars could exhibit various phenomena occurring in periodic structures, such as PBGs, negative refraction, self-collimated propagation, Zitterbewegung oscillation, unidirectional propagation, perfect tunneling, and Dirac cones [8–17]. Furthermore, since the scattering properties of the virtual pillar depend on the shape of the patch and the distance between the parallel plates, the various phenomena can be controlled in PCs composed of virtual pillars by varying the patch shape simply and tuning the distance in proper.

In this paper, the scattering properties of a virtual pillar with a circular magnetic wall for TEM modes of the waveguide are studied with numerical simulations. The simulated total scattering cross section of a virtual pillar shows that a virtual pillar mimics a PMC pillar with a radius less than that of the circular PMC patch. The photonic band structures of a triangular PC composed of the virtual pillars are investigated. Virtual pillars with a triangular lattice can exhibit PBGs. The properties of the band gaps are very similar to those of the band gaps of a triangular PC composed of infinitely long PEC cylinders for transverse magnetic (TM) modes, the magnetic field of which is parallel to the axis of the cylinder. The boundary conditions at the PEC and PEC surfaces explain well the similarity between the two different PCs. A double Dirac cone at the center of the Brillouin zone (BZ) is observed, and the wave-front conversion, which is a unique type of EM wave propagation related to an effective zero-refractive index through the triangular PC composed of virtual pillars, is demonstrated in simulation.

II. RESULTS

Figure 1(a) shows the schematic of a virtual pillar with a magnetic wall under a circular PMC patch introduced in the upper PEC plate of a parallel PEC plate waveguide. R is the radius of the PMC patch. The separation between two PEC

*topofuni@gmail.com
†cskee@gist.ac.kr

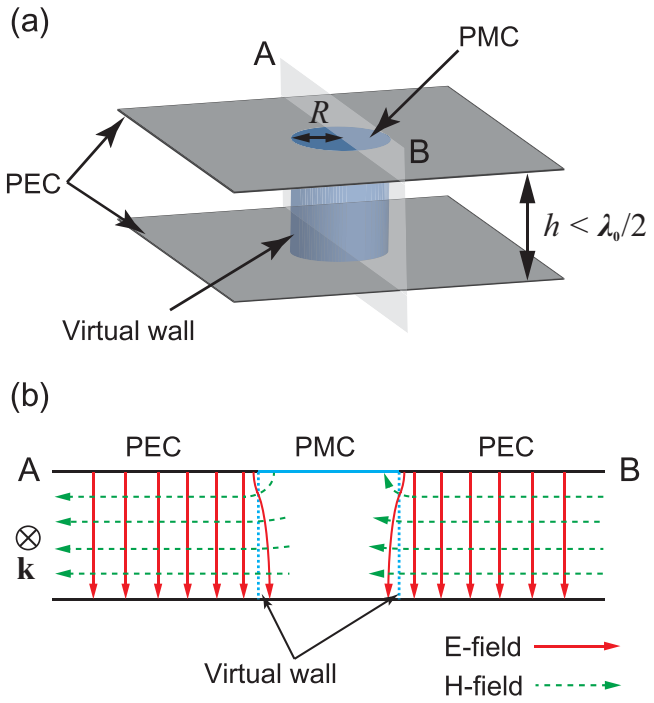

FIG. 1. (a) Schematic of a virtual pillar with a magnetic wall in a parallel perfect electric conductor plate waveguide. R is the radius of a circular perfect magnetic conductor patch and h is the distance between two perfect electric conductor plates. (b) Field distributions of a TEM mode on the cross section in (a).

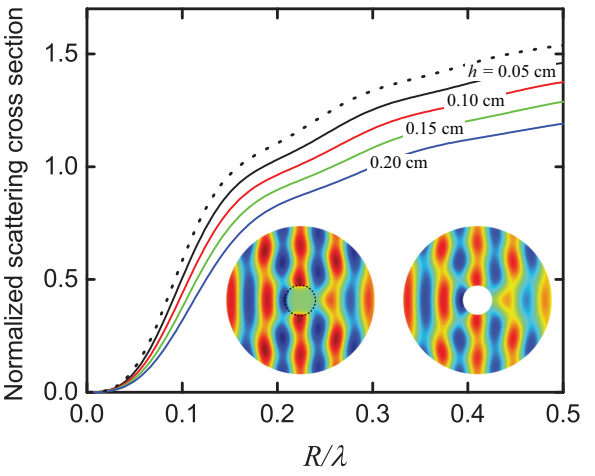

FIG. 2. Total scattering cross section of virtual pillars with different h (solid lines) and an infinitely long PMC cylinder (dotted line) as a function of R/λ, where λ is the wavelength of the EM wave and $R = 0.5$ cm. Total scattering cross sections were normalized to $2Rh$. Insets represent the spatial distributions of total fields including the incident electric field and the scattered ones from the virtual pillar with $h = 0.1$ cm (left) and PMC cylinder (right) at a frequency of 25 GHz ($R/\lambda = 0.417$). The circular dashed line and a white solid circle denote the EM virtual wall boundary and PMC cylinder, respectively.

plates h is adjusted to a value less than a half wavelength to allow only TEM modes in the waveguide. Electric fields and magnetic fields of TEM modes in the PPW are perpendicular and parallel to the plates, respectively, as illustrated in Fig. 1(b). In the PEC/PMC region, there are almost no fields, except for fringe effects around the virtual wall.

To study the scattering properties of a virtual pillar, the total scattering cross sections of pillars with different h for TEM modes are calculated. The total scattering cross section of virtual pillars with different h as a function of R/λ are represented in Fig. 2, where λ is the wavelength of an EM wave. The total scattering cross sections are normalized to $2Rh$. For comparison, the total scattering cross sections of an infinitely long PMC cylinder for a transverse electric (TE) mode with an electric field parallel to the axis of the cylinder is calculated. The radii of the virtual pillar and PMC cylinder are the same, 0.5 cm. One can see that the total scattering cross sections of virtual pillars with different h (solid lines) are much similar to that of the PMC cylinder (dotted line). Since the total scattering cross section of the PMC cylinder is only dependent on the its radius at a certain wavelength, the virtual pillar under the PMC patch mimics a PMC cylinder with a radius less than that of the patch. This is because TEM modes can slightly penetrate the virtual pillar. Because the penetration depth increases as h increases, the total scattering cross section decreases as h increases. Insets of Fig. 2 show spatial distributions of total fields of incident and scattered electric fields from the virtual pillar with $h = 0.1$ cm and PMC cylinder at a frequency of 25 GHz ($R/\lambda = 0.417$), respectively. One can see that the two field distributions are very similar. COMSOL Multiphysics based on a finite-element method is employed to calculate the total scattering cross sections and field distributions. From the boundary conditions, it is worth noting that the scattering properties of an infinitely long PMC cylinder for a TE mode are identical to those of an infinitely long PEC cylinder for a TM mode [18]. Thus, it is quite straightforward to predict that the scattering properties of the virtual pillar for a TEM mode are much similar to those of an infinitely long metallic cylinder for a TM mode. One can easily conjecture that the characteristics of a two-dimensional (2D) PC of virtual pillars for TEM modes will be similar to those of a 2D metallic PC for TM modes. To confirm the conjecture, we investigate the photonic band structures of a triangular PC composed of virtual pillars formed by introducing a triangular array of PMC patches in the upper PEC plate. COMSOL Multiphysics is employed for calculating the photonic band structures.

Figure 3(a) shows the five lowest photonic bands when $h = 0.1a$ and $R = 0.4a$, where $a = 1.0$ cm is the period of the array. The inset shows an irreducible BZ of a triangular array. Figures 3(b)–3(e) show the electric field distributions of the four lowest eigenmodes with frequencies of 0.9786 (29.338 GHz), 1.0157 (30.451 GHz), 1.0165 (30.475 GHz), and 1.5165 (45.463 GHz) at the Γ point, respectively. One can see that the first mode is a hexapolar mode, the second a quadrupolar mode, the third a quadrupolar mode, and the fourth a dipolar mode. The field distributions show that TEM modes can slightly penetrate the virtual pillar, similar to how TM modes penetrate a metallic cylinder. The band structures and field distribution are much similar to those of a triangular metallic PC for the TM mode reported previously [19]. Figure 4 shows photonic band gaps (G_1, G_2, and G_3) of the triangular PC as a function of R/a. G_1 is between the second band at the Γ point and the third band at the K point. G_2 is between the third and fourth bands at

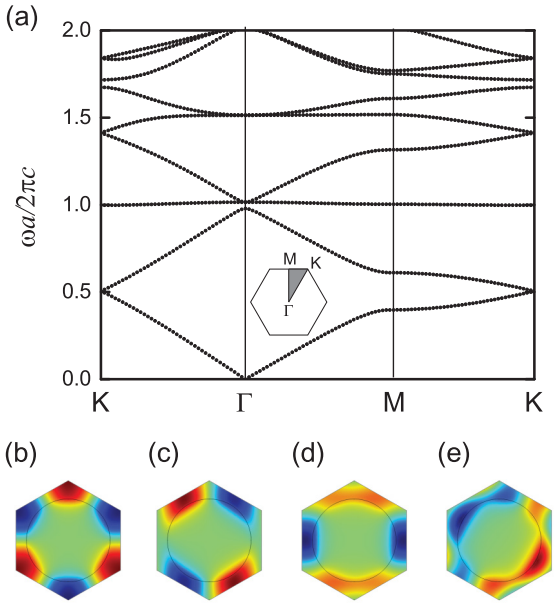

FIG. 3. (a) Photonic band structure of a triangular photonic crystal composed of virtual pillars when $h = 0.1a$ and $R = 0.4a$, where $a = 1.0$ cm is the period of the array. The frequency ω is normalized by $2\pi c/a$, where c is the speed of light in free space. The inset shows an irreducible Brillouin zone of a triangular array. Electric field distribution of the four lowest eigenmodes with frequencies of (b) 0.9786 (29.338 GHz), (c) 1.0157 (30.451 GHz), (d) 1.0165 (30.475 GHz), and (e) 1.5165 (45.463 GHz) at the Γ point. The circle denotes the EM virtual wall boundary.

the Γ point. G_3 is between the sixth and seventh bands at the K point when R/a is smaller than 0.44. From $R/a = 0.44$ to 0.5, G_3 is between the sixth band at the K point and seventh band at the Γ point. Usually, a PBG is open at a lower R/a and closed at a higher R/a because the band gap is due to the interference

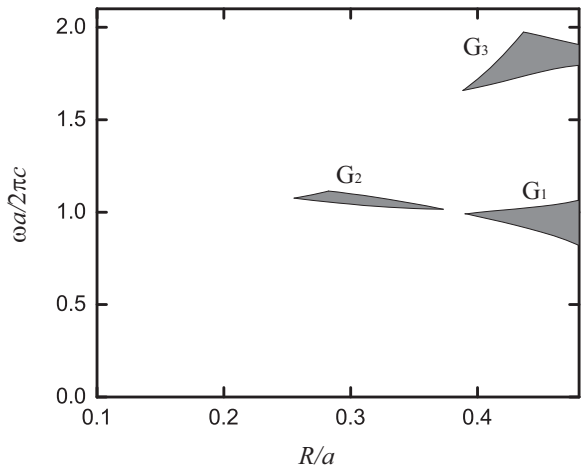

FIG. 4. Photonic band gaps (G_1, G_2, and G_3) as a function of R/a. G_1 is between the second band at the Γ point and the third band at the K point. G_2 is between the third and fourth bands at the Γ point. G_3 is between the sixth and seventh bands at the K point when R/a is smaller than 0.44. From $R/a = 0.44$ to 0.5, G_3 is between the sixth band at the K point and seventh band at the Γ point.

of EM waves multiply reflected from interfaces between composites of a PC. However, interestingly, G_1 increases as R/a increases. The unusual dependence of the band gap on R/a was also observed in the PCs of PEC cylinders [20]. At the high filling fraction of the PEC cylinder, a cavity is formed between the nearest neighbor cylinders. The coupling between the resonant eigenmodes of neighboring cavities creates the bands of modes propagating through the cavities. The gap between the bands increases when the filling fraction increases because the cavity size decreases as the filling fraction increases [21].

One of the interesting properties of PCs is its unusual dispersion that gives rise to unique types of EM wave propagation such as negative refraction and self-collimated beam propagation. It has been reported that PCs can have a linear dispersion relation, called Dirac cone dispersion, on the BZ boundary as well as the BZ center [12,22]. The observation of Dirac cones at the Γ point has attracted much attention because the PCs with Dirac cones at the Γ point can act as zero-refractive-index materials to allow uncommon types of EM wave propagation such as cloaking and unidirectional transmission [15]. Recently, the double Dirac cone degeneracy at the Γ point was predicted in triangular-lattice metamaterials and dielectric PCs [23,24]. The double Dirac cone, which is a pair of two identical and overlapping Dirac cones, is realized by utilizing a fourfold accidental degeneracy, which is the accidental degeneracy of the doubly degenerate dipolar and quadrupolar modes.

It is noteworthy that a triangular PC of virtual pillars exhibits the double Dirac cone at the Γ point. Figure 5(a) shows the photonic band structures of the triangular PC when $R/a = 0.25239$. One can see that four bands linearly intersect at a fourfold degenerate point A at the Γ point. The enlarged view of the band structure around the A point in Fig. 5(b) shows that two identical and overlapping Dirac cones form a double Dirac cone. It has been demonstrated that the linear dispersion calculated numerically using COMSOL Multiphysics agrees well with that predicted theoretically using $\vec{k} \cdot \vec{p}$ method [25]. The slopes of the linear dispersions estimated from the numerical calculations are approximately $\pm 0.505c$. The solid lines denote the linear dispersions of $\omega = \pm 0.505ck$. The field distributions of doubly degenerate dipolar and quadrupolar modes at the A point are represented in Figs. 5(c)–5(f), respectively. The unique types of EM wave propagation caused by effective zero-refractive index, such as wave-front shaping, unidirectional transmission, and perfect tunneling of TEM modes through the triangular PC composed of virtual pillars is predicted reasonably at the frequency of the A point [24]. In order to give evidence of the double Dirac cone of the virtual pillar PC, the wave-front shaping through the triangular PC composed of virtual pillars is examined at the Dirac point frequency. Figure 5(g) shows that the wave front of an incident Gaussian wave with the Dirac point frequency, 1.0770 (32.289 GHz), is clearly reshaped to that of a plane wave through a slab of triangular PC of virtual pillars. Other EM propagation phenomena occurring in zero-index media could be simulated in the triangular PC.

A high impedance surface can mimic a PMC surface in practice because a magnetic field has a node at the surface, while an electric field has an antinode. The high impedance surface has been implemented by a metallic array printed

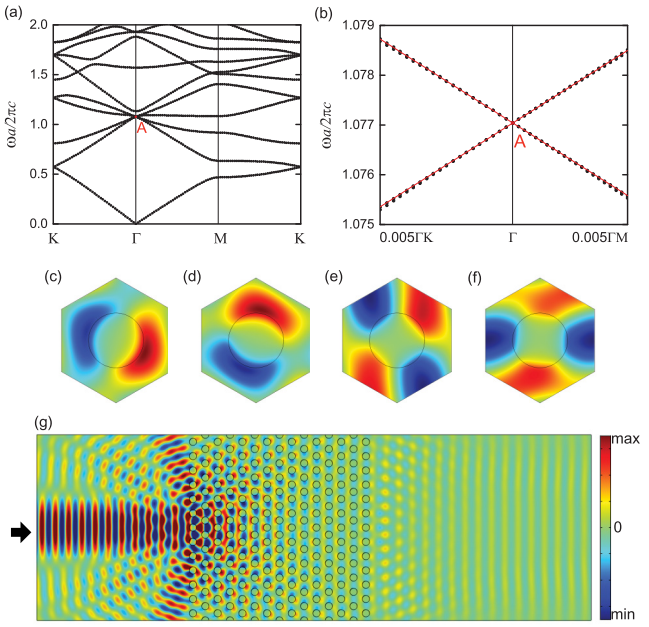

FIG. 5. (a) Photonic band structures of the triangular PC when $R/a = 0.25293$. (b) Enlarged view of the band structure around the A point. The solid lines denote the linear dispersions of $\omega = \pm 0.505ck$. (c)–(f) The field distributions of doubly degenerate dipolar and quadrupolar modes at the A point. The circle denotes the EM virtual wall boundary. (g) Electric field distributions produced by a Gaussian wave passing through a slab of triangular PC of virtual pillars at the double Dirac point frequency, 1.0770 (32.289 GHz). An incident Gaussian beam with a width of $2a$ and a $7\sqrt{3}a \times 13a$ slab of the PC are employed in the simulation.

on a grounded dielectric substrate and connected vias to the ground [1]. It has been reported that a planar PBG structure metallic arrays printed on the dielectric substrate can also mimic a PMC surface [2]. However, it is necessary to design broadband high impedance surfaces and wide PBG planar structures because the high impedance and PBG frequency ranges of the previous structures are narrow. Our triangular PC of virtual pillars could be implemented by properly designed broadband high impedance surfaces and wide PBG planar structures. Experimental demonstration of the wave-front shaping through the triangular PC composed of virtual pillars will be an interesting challenge.

III. CONCLUSION

In conclusion, we demonstrated that introducing a PMC patch in the upper PEC plate of a parallel PEC plate waveguide creates a virtual pillar mimicking a PMC cylinder in simulation. The photonic band structures of triangular PCs composed of virtual pillars for TEM modes of the waveguide are investigated. The characteristics of eigenmodes and band gaps are very similar to those of a triangular PC of PEC cylinders for TM modes because of boundary conditions at PEC and PMC surfaces. The triangular PC composed of virtual pillars can have a double Dirac cone at the Γ point. The wave-front reshaping due to the effective zero-refractive index at the Dirac cone frequency is numerically demonstrated.

ACKNOWLEDGMENTS

This work was supported by the GIST Research Institute (GRI) in 2016 and the Basic Science Research Program through the National Research Foundation of Korea (NRF) funded by the Ministry of Education, Science and Technology (No. NRF-2015R1D1A1A01060180 and NRF-2011-357-C00042).

[1] D. Sievenpiper, L. Zhang, R. F. J. Brods, N. G. Alexopolous, and E. Yablonovitch, IEEE Trans. Microw. Theory Tech. **47**, 2059 (1999).
[2] F.-R. Yang, K.-P. Ma, Y. Qian, and T. Itoh, IEEE Trans. Microw. Theory Tech. **47**, 2092 (1999).
[3] D. J. Kern, D. H. Werner, A. Monorchio, L. Lanuzza, and M. J. Wilhelm, IEEE Trans. Antennas Propag. **53**, 8 (2005).
[4] M. Grau, R. Serra, and J. Parron, Electron. Lett. **50**, 1340 (2014).
[5] J. B. Pendry, L. Martin-Moreno, and F. J. Garcia-Vidal, Science **305**, 847 (2004).
[6] A. P. Hibbins, B. R. Evans, and J. R. Sambles, Science **308**, 670 (2005).
[7] L. Liu, Z. Li, C. Gu, P. Ning, B. Xu, Z. Niu, and Y. Zhao, Opt. Express **22**, 10675 (2014).
[8] J. D. Joannopoulos, S. G. Johnson, J. N. Winn, and R. D. Meade, *Photonic Crystals: Molding the Flow of Light* (Princeton University Press, Princeton, NJ, 2008).
[9] S. Foteinopoulou, E. N. Economou, and C. M. Soukoulis, Phys. Rev. Lett. **90**, 107402 (2003).
[10] S.-G. Lee, J.-M. Park, and C.-S. Kee, Opt. Express **22**, 28954 (2014).
[11] K.-J. Kim, J.-E. Kim, H. Y. Park, Y.-H. Lee, S.-H. Kim, S.-G. Lee, and C.-S. Kee, Opt. Express **22**, 4050 (2014).
[12] X. Zhang, Phys. Rev. Lett. **100**, 113903 (2008).
[13] T. Ochiai and M. Onoda, Phys. Rev. B **80**, 155103 (2009).
[14] F. D. M. Haldane and S. Raghu, Phys. Rev. Lett. **100**, 013904 (2008).
[15] X. Huang, Y. Lai, Z. H. Hang, H. Zheng, and C. T. Chan, Nat. Mater. **10**, 582 (2011).
[16] M. Bellec, U. Kuhl, G. Montambaux, and F. Mortessagne, Phys. Rev. Lett. **110**, 033902 (2013).
[17] Y. Wu, Opt. Express **22**, 1906 (2014).
[18] D. M. Pozar, *Microwave Engineering* (Wiley, NewYork, 2004).
[19] E. Degirmenci and P. Landais, Appl. Opt. **52**, 7367 (2013).
[20] E. I. Smirnova, C. Chen, M. A. Shapiro, J. R. Sirigiri, and R. J. Temkin, J. Appl. Phys. **91**, 960 (2002).
[21] B. Reinhard, G. Torosyan, and R. Beigang, Appl. Phys. Lett. **92**, 201107 (2008).
[22] F. Liu, X. Huang, and C. T. Chan, Appl. Phys. Lett. **100**, 071911 (2012).
[23] K. Sakoda, Opt. Express **20**, 9925 (2012).
[24] Y. Li and J. Mei, Opt. Express **23**, 12089 (2015).
[25] J. Mei, Y. Wu, C. T. Chan, and Z.-Q. Zhang, Phys. Rev. B **86**, 035141 (2012).